ELSEVIER

Available online at www.sciencedirect.com

SCIENCE DIRECT®

Earth and Planetary Science Letters 217 (2003) 97–109

EPSL

www.elsevier.com/locate/epsl

Tectonic evolution of the Antarctic–Phoenix plate system since 15 Ma

Graeme Eagles *

Alfred Wegener Institute for Polar and Marine Research, Columbusstraße, D-27568 Bremerhaven, Germany

Received 4 July 2003; received in revised form 1 September 2003; accepted 10 October 2003

Abstract

Joint inversion of magnetic isochron and fracture zone data from the extinct Antarctic–Phoenix spreading system in SW Drake Passage yields seven new finite reconstruction poles. The inversion results are very well constrained for such a short length of plate boundary. Although this is partly because the finite poles are located close to the reconstructed region, the optimum use of fracture zone identifications from satellite-derived free-air gravity data is also important – as the stability of stage poles throughout the short intervals in the model affirms. The model results describe a well-organised spreading system since magnetic anomaly chron C5AD (~15 Ma) in which the Phoenix plate rotated about stage poles nearby to the southwest. Stage pole locations are broadly consistent with a hypothesis of pivoting subduction as the driving force of Phoenix plate movement, and there is some evidence in the progression of stage poles for late stage movement of the subduction pivot in response to the changing azimuth of the subduction zone at which the Phoenix plate was being consumed. The model kinematics alone provide no unequivocal support for previous interpretations of disruption of the subducted part of the Phoenix plate. The very latest stages of spreading saw falling spreading rates between magnetic anomaly chrons C4 (~8.1 Ma) and C2A (~3.3 Ma) when the Antarctic–Phoenix Ridge became extinct. This is consistent with an increase in shear stress across the plate bounding Shackleton Fracture Zone due to a plate reorganisation in the neighbouring Scotia Sea following the cessation of spreading on the West Scotia Ridge.

Keywords: Antarctica; Drake Passage; fracture zones; plate motion; seafloor spreading; subduction

1. Introduction

There is a need for an accurate set of parameters describing the Neogene–Recent plate tectonic history of the Antarctic–Phoenix spreading system. The Phoenix plate has been treated in the past as a laboratory for the study of plate tectonic driving forces [1] via the study of seafloor spreading rate changes revealed in magnetic anomaly profiles [1,2]. An inversion that fits conjugate magnetic anomaly identifications together is a powerful technique to identify discrepancies in identifications of anomalies on profiles and generate estimates of spreading rates. In Section 6 I make a comparison to those earlier studies in order to comment on the plate dynamics of the region.

* Tel.: +49-471-48311213; Fax: +49-471-48311149.
E-mail address: geagles@awi-bremerhaven.de (G. Eagles).

0012-821X/03/$ – see front matter © 2003 Elsevier B.V. All rights reserved.
doi:10.1016/S0012-821X(03)00584-3

Secondly, understanding the Phoenix plate's movements in the past is an important and necessary step towards reconstructions of Drake Passage – one of the final links in Neogene completion of a deep-water circumpolar pathway at high latitudes. The ensuing Antarctic Circumpolar Current is a major feature of Neogene climate that may have been linked to the onset of Antarctic glaciation [3].

Finally, the system was a key link in the late Tertiary global plate circuit, as no subduction has occurred at its NE boundary facing the Atlantic, the Shackleton Fracture Zone (SFZ). This setting is in contrast to most of the rest of the Pacific Ocean that is ringed by subduction zones that make it difficult to reconcile discrepancies between the Pacific and Indo-Atlantic plate circuits. These discrepancies give rise to a disagreement with the notion of fixity of the hotspots with respect to one another that challenges ideas of the hotspots' role in the mantle.

2. Tectonic setting

The Antarctic–Phoenix Ridge (also called Phoenix Ridge) consists of three extinct spreading ridge segments west of the northern Antarctic Peninsula (Fig. 1) and southwest of the Scotia Sea. These segments separated the Phoenix (sometimes called Aluk, or Drake) plate on its SE flank from the Antarctic plate on its NW flank [1]. Hence, the ridge also goes under other names. The ridge's initiation followed late Cretaceous to early Tertiary times when the Phoenix plate had divergent boundaries with the Bellingshausen and Pacific plates in the SW Pacific Ocean. The Bellingshausen plate fused with the Antarctic plate at chron C27 (~61 Ma) [5], and at chron C21 (~47 Ma) the Phoenix part of the last Pacific–Phoenix spreading corridor was captured by the Antarctic plate as a result of Pacific–Antarctic Ridge propagation [6]. The resulting Antarctic–Phoenix Ridge, between the Phoenix and Antarctic plates, was situated to the northwest of a subduction zone at the margin of the Antarctic Peninsula, where the Phoenix plate was subducting beneath the Antarctic plate. Ridge-crest segments periodically obliquely collided with the subduction zone in this setting; the earliest collided in the southwest and subsequent ones successively in the spreading corridors to the northeast. The last collisions occurred at ~62°S–63°S on the margin around chron C3A (~6.5 Ma) [1]. Spreading on the Antarctic–Phoenix Ridge stopped around anomaly C2A (~3.3 Ma) [2], leaving only a small remnant of the Phoenix plate unsubducted, and this remnant was incorporated into the Antarctic plate.

The southeastern boundary of this incorporated remnant is the South Shetland Trench; the northeastern boundary is the SFZ that separated it from the west Scotia Sea. The west Scotia Sea north of the SFZ consisted of two plates diverging at the slow-spreading West Scotia Ridge until some time between chrons C4 and C3A (~8–6.5 Ma) [7,8], when the West Scotia Ridge failed and a single Scotia plate formed north of the SFZ. The SFZ is likely to have formed a plate boundary between the Antarctic and Scotia plates since incorporation of the Phoenix plate into the Antarctic plate at anomaly C2A [2,9]. Since that time, the entire region has been the site of E–W compressive stress [9], which may include continued shortening and subduction at the South Shetland Trench.

The short length of ridge from which conjugate magnetic isochron data are available for reconstructions, and the very variable coverage of these isochron data, might be expected to provide unstable and poorly constrained results in isochron-fitting procedures intended to determine reconstruction parameters. Seafloor created during the spreading process has left fracture zones (FZs) south of the remaining fragment of the Phoenix plate that were created in the same setting as those further north. By using these data, the range of colatitudes of data available for reconstruction of Antarctic–Phoenix spreading since chron C5AD (~15 Ma) could be doubled. In this paper, I present a new set of finite reconstruction parameters for Antarctic–Phoenix spreading since chron C5AD based on joint inversion of magnetic anomaly isochron and altimeter-derived free-air gravity FZ data from the remaining conjugated segments, as well as FZ data from the unconjugated segments further south.

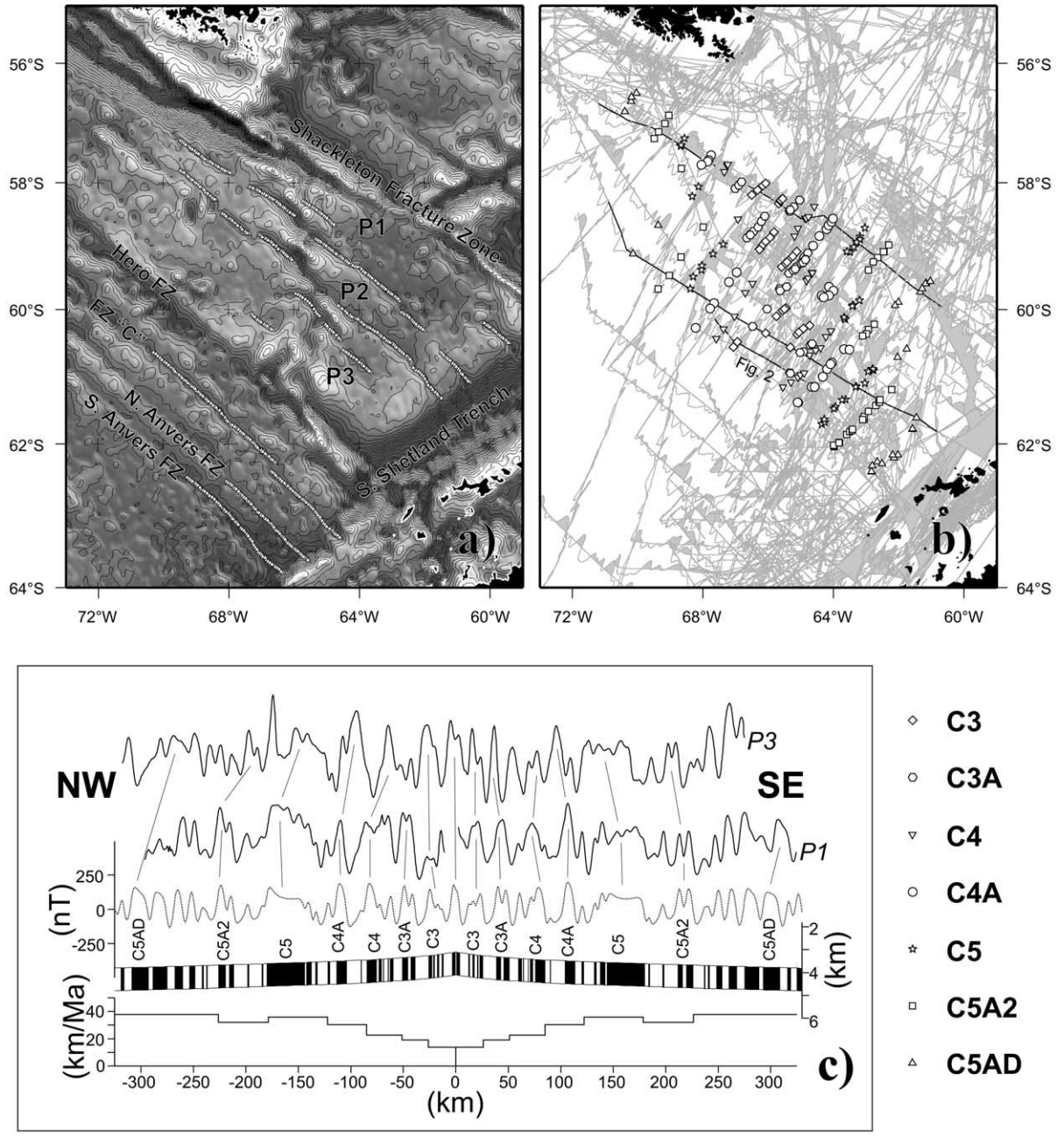

Fig. 1. (a) Gridded gravity anomalies and picks (triangle symbols) of FZ crossings. (b) Gridded and along-track magnetic anomalies, and magnetic reversal chron picks (white symbols, with key bottom right). (c) Example magnetic profiles in segments P1 and P3, and a synthetic profile (dotted line), generated using a standard thermal subsidence curve (bottom) as the top surface of a 1 km thick source layer, the timescale of [4], and spreading rates generated from the inversion results for segment P1. No ridge jumps or spreading asymmetry are modelled. Effective susceptibility of 0.005, profiles projected onto 130°, model geomagnetic inclination and declination were taken from IGRF80, for the region in 1990.

3. Method

Seafloor spreading data from the Antarctic–Phoenix Ridge and its flanks are used to calculate finite rotation poles using the technique of Nankivell [10]. This technique is a refinement and extension of that of Shaw and Cande [11], but for the conjugate isochron-fitting exercise described here, the two can be considered identical. These techniques are founded in the work of Shaw [12] who realised a technique for fitting FZ picks to model flowlines that is more suited to their use in modelling seafloor spreading as a continuous process than the widely used technique of Hellinger [13]. These techniques [10–12] are specifically more suitable to model FZs because they do so by treating them as segments of small circles, rather than great circles, because they explicitly account for the finite offset of FZs at transform faults, and because they can make use of all available FZ pick data.

3.1. Data

Antarctic–Phoenix magnetic reversal anomaly isochrons formed during seafloor spreading have been modelled in the past [1,2,8,14]. Before chrons C3A/C3, the modelling is a reasonably simple process as the spreading rate was mostly fast (>50 km/Myr full rate) and produced coherent, well-defined anomalies. The pattern in many corridors is complicated by short-range ridge jumps, usually away from the trench, as old as anomaly C8, as well as variable spreading asymmetry that can be demonstrated in the surviving three ridge segments (labelled P1, P2 and P3, from north to south) and may reach 10% in favour of the Phoenix flank [1,2]. My anomaly picks do not deviate significantly from these already published models and, to avoid duplication of profile data, only two examples of long profiles are shown in Fig. 1c. After chron C3, spreading rates are slower and the axial region's topography often confuses profiles, which has made it difficult to identify sequences of reversals about P1 and P3 where recorded anomaly sequences are incoherent. Two different interpretations of C3 and post-C3 anomalies are described in the literature, but they differ significantly only in the southern part of segment P3. The earlier of these interpretations places conjugate anomalies C3 and younger very close together in southernmost P3 [1]. It is also possible to interpret more widely spaced young conjugate anomalies in southernmost P3 (Fig. 2) using the model of a coherent, symmetrical set of profiles [2], over the axis in P2, as a guide. To

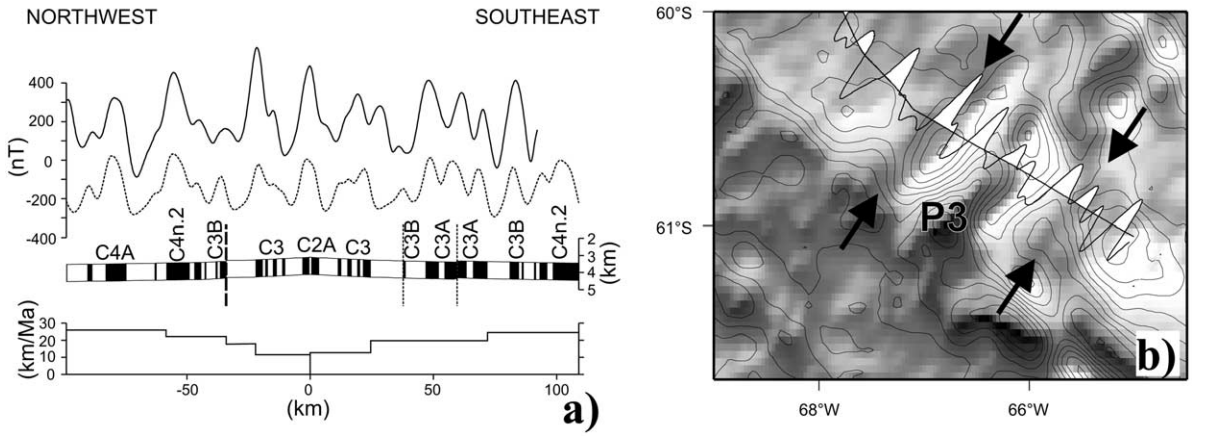

Fig. 2. (a) Detailed model spreading in southern segment P3, compared to a ship track profile. Parameters the same as in Fig. 1, except that the rates and predicted bathymetry have been changed to fit the sequence more accurately, including a northwestwards ridge jump of 21 km at 5.9 Ma and post-10 Ma asymmetry favouring the Phoenix flank by 5%. Thick dashed vertical line: former location of missing sequence; thin dashed vertical lines: extents of sequence transferred to Phoenix flank by jump. (b) The modelled profile overlaid on free-air gravity anomalies. Isochron-parallel anomalies (between arrows) are ridge jump scars.

make this interpretation requires a short ridge jump towards the Antarctic flank, at chron C3An.1y. The jump defines an axis of post-C3 symmetry that is between more widely spaced post-C3 conjugate anomalies, that falls within the free-air anomaly low marking the extinct median valley in P3, and that explains extra reversals on the Phoenix plate flank (Fig. 2). I plotted all available magnetic anomaly profiles from the British Antarctic Survey's marine geophysics database as along-track wiggles, and overlaid them on a gridded representation of magnetic anomalies in the Antarctic–Phoenix Ridge region to aid interpretation of high angle ship tracks. On-screen digitising of the interpretations yielded 187 crossings of anomalies labelled C3, C3A, C4, C4A, C5, C5A2, and C5AD (see Table 1 for ages). I also produced a similar data set, but using the interpretation of closely spaced young conjugate anomalies in P3. Although older anomalies are present on both flanks of the system in P1 and P2, due to sparse coverage by ship tracks they do not form useful sets of conjugate identifications.

Segments P1, P2 and P3 are defined on the basis of extinct medium offset transform faults that have left FZ traces. Magnetic anomaly offsets require that there must be further FZ traces to the southwest, defining further spreading corridors where the ridge crests cannot be defined due to collisions with the Antarctic Peninsula. The four most northerly of these extra FZs (the Hero, 'C', N. Anvers and S. Anvers FZs; Fig. 1) have parts that are younger than anomaly C5AD, and hence could be of use here. Although this part of the Antarctic Peninsula's margin is heavily sedimented, the narrow, straight free-air gravity anomalies probably also express the underlying tectonic fabric of the sedimented seafloor, as their coincidence with occasional magnetic anomaly reversals suggests. I omitted data from the Hero FZ in view of the possibility of former non-strike-slip motions across its very long transform offset. I also split FZ 'C' into two separate lengths at an offset near 66.3°W, 62.1°S. This offset is seen neither in GLORIA data [15] nor along the other FZs in the system, and splitting 'C' here ensures that the offset has no influence over the model. As mentioned above, and in [2], the ridge crest in P3 has been affected by some small-scale ridge jumps, subdividing the segment since chron C4, and leaving some short FZ traces that offset magnetic anomaly identifications. A ridge jump also seems to have removed an older offset in P1, as a gravity trough and offset of anomaly determinations older than C5AD terminate at that chron on the Phoenix flank. All of the FZ features that form a large co-polar set, as well as the fossil transform faults, which are of use in calculation of the most recent reconstruction pole, were digitised directly from a satellite-derived free-air gravity grid as picks at ~5 km separation (Fig. 1a; [16]). This process produces 496 FZ data, and 75 from the transforms.

3.2. Data uncertainties

Uncertainties in the position of magnetic picks

Table 1
Finite poles for Phoenix with respect to Antarctic plate reconstructions

Reconstruction parameters						Confidence ellipsoids			
Label	Chron	Age	Lat	Lon	Angle	Ax1	Ax2	Ax3	Az
C3	3n.4no	5.23	−68.07	−91.96	1.83	0.22	0.08	0.02	17.61
C3A	3An.2no	6.57	−69.21	−97.32	3.07	0.75	0.05	0.01	19.14
C4	4n.2no	8.07	−68.98	−90.41	5.85	0.30	0.03	0.02	26.82
C4A	4Ar.1no	9.31	−69.77	−92.17	7.94	0.19	0.02	0.01	26.25
C5	5n.2no	10.95	−69.98	−94.12	11.23	0.15	0.02	0.01	23.31
C5A2	5An.2no	12.40	−70.23	−96.68	13.38	0.13	0.01	0.01	20.60
C5AD	5ADno	14.61	−70.02	−94.97	18.94	0.36	0.02	0.01	17.97

Magnetic chrons are from the timescale of [4]. Latitude, longitude and angle are in degrees north, east, anticlockwise, respectively. Ax1, Ax2, Ax3 and Az refer to the three axes of the 95% confidence ellipsoid, in great circle degrees/2.79, and its orientation in degrees.

due to normal skewness are negligible due to the high magnetic inclination at high latitudes, and I have done nothing to correct for it. The uncertainty due to the digitising process, based on computed errors in geo-referencing the along-track wiggle plot, is also negligible. The principal source of uncertainty in the magnetic data has been treated as due either to navigational uncertainty [17] or to uncertainties in knowledge of the distance between a ship's GPS receiver and magnetometer and in identifying precise points in magnetic field intensity profiles [18]. Uncertainties based on navigational considerations are predicted as on average between 4.4 km and 6.7 km for the region, depending on estimates of the accuracy of Transit satellite navigation [8]. The uncertainty in the position of FZ troughs picked from satellite altimetry data, determined with respect to well-fixed ship soundings at the Kane FZ, has been shown to be $\sim$5 km [19]. Uncertainties based on difficulty in interpreting along-track anomalies and magnetometer–receiver spacing may be in the region of 2.5–3.5 km [18]. In practice, the data uncertainty is estimated using the standard deviations of the residual populations generated by the inversion process. Fig. 2 shows cross-plots of quantiles of the residuals and of a known normal distribution (quantile–quantile, or Q–Q plots [10,11]) at the end of the inversion, whose gradients give an indication of the populations' standard deviations. The estimated overall uncertainties are 2.8 km for isochron and 1.5 km for FZ data; both values are smaller than uncertainties from consideration of likely navigational errors. The isochron value is more consistent with uncertainty being the result of interpretation noise [18] and the FZ value may in part be due to improvements in the resolution of satellite-derived free-air anomalies since the Kane FZ study [19].

3.3. Generating the solution and confidence regions

If certain assumptions are justifiable, this approach will converge within appropriate limits (i.e. those for the least accurate of all the data) and is able to illustrate the effects of data uncertainty as comparable confidence regions to the rigorous and robust confidence regions of the widely used two-plate fit Chang/Hellinger [20,21] technique. The inversion equation is linearised in order to be able to derive the covariances that define the confidence regions by using partial derivatives after one-plate fitting of isochron data; one plate is held fixed for each isochron in each spreading corridor and its data define a target for rotation of data from the other plate. Hence, an important assumption for estimating confidence regions using uncertainties is that the distributions of data uncertainties on the fixed and moving plates are similar [20]. This assumption is valid with satellite free-air anomaly data, and is likely to be valid with the magnetic data used here, as many of the individual ship tracks sampled both plates over a short length of time. The second important assumption is of a normal distribution of uncertainties in all the data contributing to the inversion. This assumption is necessary because the covariances used to calculate the confidence regions are directly derived from the distribution of residuals in the inversion equation, rather than using a priori assigned uncertainties. This assumption is never fully met, because of the presence of outliers in the residual populations, but the populations can be censored in order to disregard the outliers in the calculation of covariances. Q–Q plots (Fig. 3) show where the normally distributed majority of the residuals is disrupted by the presence of outliers, and a suitable overall censoring criterion can be chosen.

I first performed 10 iterations with all the data in order to approach the general region of the solution. This was done with extra weighting given to the isochron data, in order to take account of the greater number of FZ data. Afterwards I replaced this bias with Nankivell's [10] weighting scheme and censored some of the data, before iterating to convergence. The limits of censoring for this inversion were set at ± 1.0 and ± 1.5 standard deviations of the populations of isochron and FZ residuals, respectively. In practice this means that 60% of the magnetic and 71% of the FZ data have an influence on the solution after censoring at convergence. Solutions with censoring set at ± 3.0 standard deviations of all data types, in which $>95\%$ of the data have an influ-

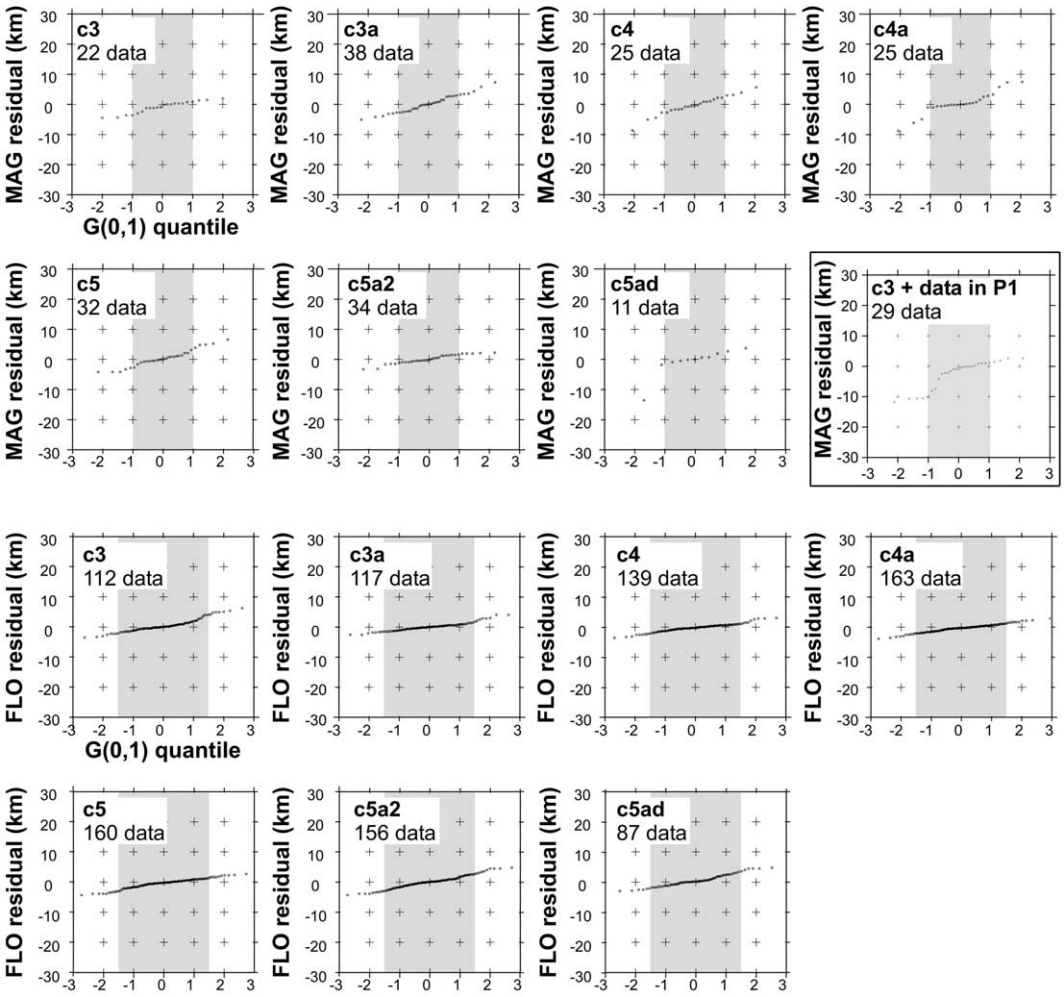

Fig. 3. Q–Q plots for magnetic isochron and FZ data residuals for each of the modelled finite poles. The normally distributed parts of the residual populations plot as a straight line, and this is disrupted by the presence of outliers. The shaded areas highlight those limits between which data are permitted to have an influence on the solutions (± 1 standard deviation for FZ data and ± 1.5 standard deviations for magnetic data). A Q–Q plot of C3 residuals for an inversion including data from segment P1 (see main text) is also shown.

ence on the solution, are very similar to the solution presented here.

4. Inversion with closely spaced conjugate C3 picks in P3

Only the results of the inversion using widely spaced young conjugate anomalies in P3 are discussed in detail in this paper. This is because an inversion with the closely spaced conjugate C3 anomalies in southern P3 yields good fits only in segment P3 itself. The inversion produces C3 misfits that become increasingly large northwards, until in segments P2 and P1 rotated C3 picks miss their targets by more than 70 km and 100 km, respectively. This is an illustration of a very close pole for chron C3, that has been 'captured' by strong curvature in the C3 target figure defined in segment P3 due to the close spacing of picks in the south. Persisting with the closely spaced conjugate C3 interpretation of [1] requires the exis-

tence of a third plate, or huge non-rigidity, in the Antarctic–Phoenix region, after this time. There is no independent evidence for either of these possibilities, and hence I prefer an interpretation of widely spaced conjugate C3 picks in P3, for which the necessary ridge jump is supported by independent evidence (Fig. 2).

5. Results of inversion with widely spaced conjugate C3 picks in P3

Picks of anomaly C3 in segment P1 were not used to generate the end solution because they give rise to a modest set of outliers. Fig. 4a shows the relative importances of data in the inversion [10,22]. The size of each circle symbol is proportional to the importance to the stability of the solution of the datum at its centre. The magnetic isochron picks, of which there are fewer than FZ picks, are accordingly more important as individuals. For similar reasons, the most important of the magnetic picks are those from the sparsest-populated segments of the isochron population (for instance, C5AD on the Antarctic flank in P3). Including the FZ data, overall a wide spread and large number of the data contribute evenly to the solution, showing that the solution is a good description of them all. Fig. 4b shows visual fits of the data to the model that reinforce this notion qualitatively.

Table 1 and Fig. 5 show the solution finite

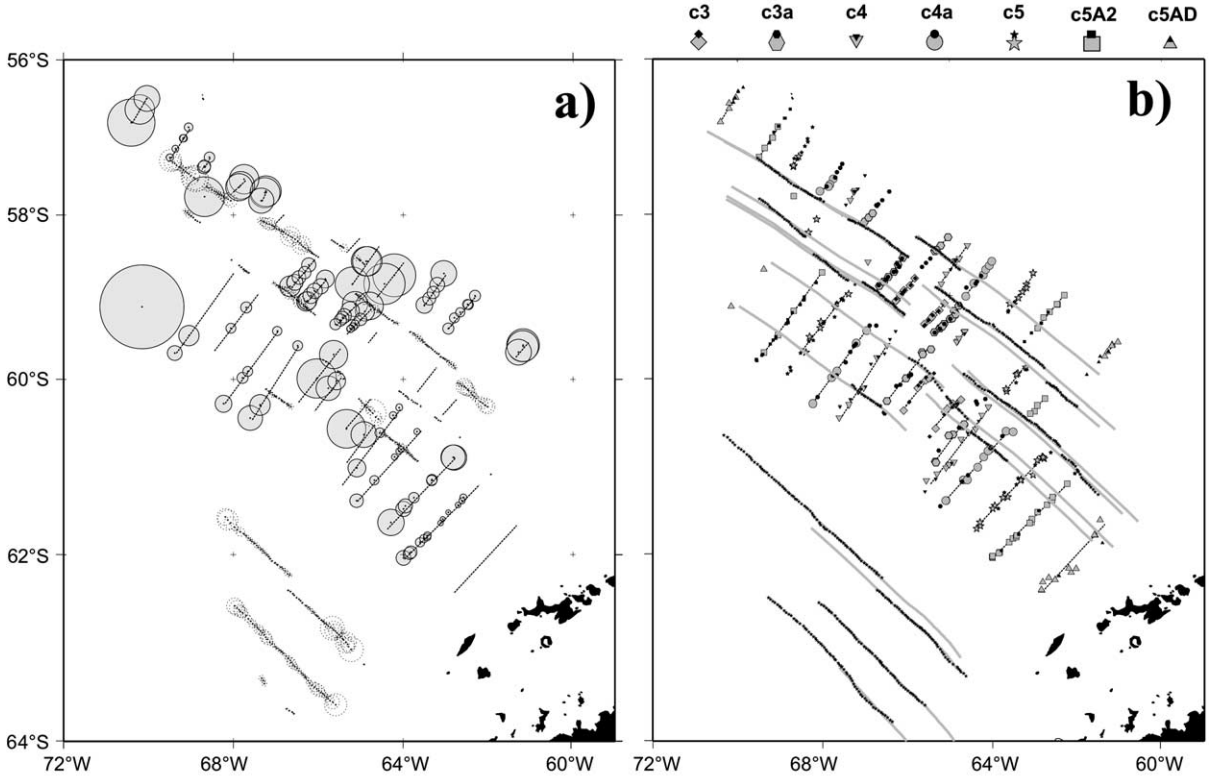

Fig. 4. (a) Data importances. Filled circles: importances for magnetic isochron data; unfilled circles: data importances for FZ data. (b) Fits of data in the model. Black dashed lines: segments of target great circles for one-plate fitting based on unrotated magnetic isochron data (filled grey symbols); small black symbols: rotated magnetic isochron data; grey lines: model flowlines; black star symbols: FZ data.

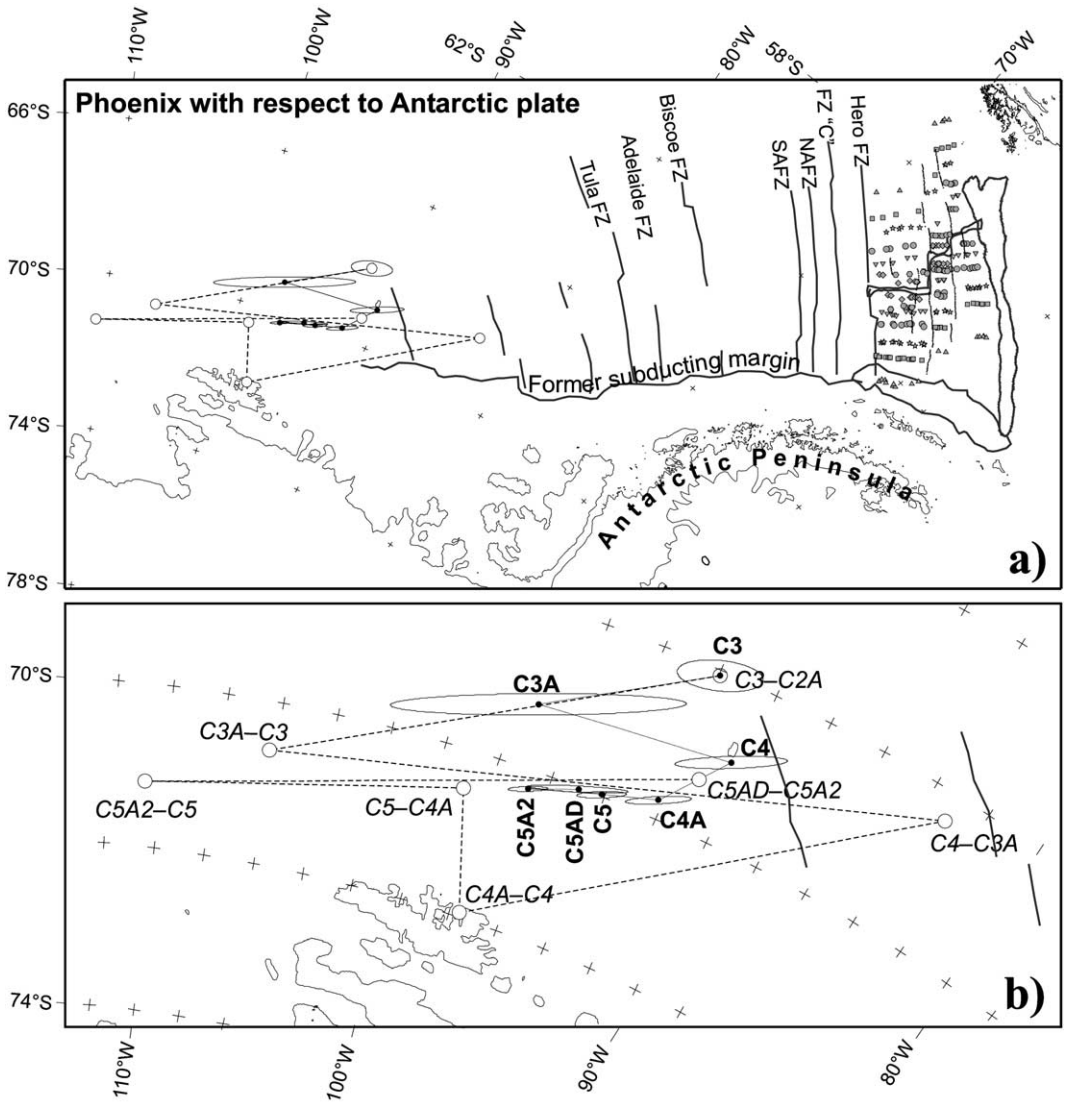

Fig. 5. (a) Finite reconstruction poles for Phoenix with respect to Antarctic plate reconstructions, and their two-dimensional 95% confidence ellipses, in their regional context, Phoenix–Antarctic spreading regime symbols as for Figs. 1b and 3a. (b) The mapped finite and stage poles and confidence regions enlarged and labelled for clarity. Large circle symbols connected by dotted line: stage poles calculated from the finite poles (see Table 2).

poles (reconstruction poles to extinction) and estimated confidence ellipses. The set of poles is closely clustered and each falls within a tight confidence region, given the short length of boundary available for the inversion. A large part of the reason for the tight confidence regions is undoubtedly the proximity of the data to the region of the solution poles, meaning there is substantial unique curvature in the target figures. The clustering of the poles, using data taken from such a short length of plate boundary is more likely a result of the continuous nature of the FZ modelling technique and the numerous FZ data, and this must also contribute to the tightness of the

Table 2
Stage poles for movement of the Phoenix plate in the Antarctic plate reference frame, calculated from the finite poles in Table 1

Interval	Duration (Myr)	Lat	Lon	Angle
C3–extinction	~1.93	−68.15	−92.18	0.89
C3A–C3	1.34	−70.44	−105.64	0.60
C4–C3A	1.50	−68.47	−83.53	1.41
C4A–C4	1.24	−71.95	−97.50	1.05
C5–C4A	1.64	−70.49	−99.11	1.64
C5A2–C5	1.45	−71.04	−105.47	1.17
C5AD–C5A2	2.21	−69.49	−92.39	2.68
C6A–C5C[a]	~4.4	−66.8	−79.2	6.8

Latitude, longitude and angle are in degrees north, east, anticlockwise, respectively.
[a] The C6A–C5C stage pole is from [1].

confidence regions. To illustrate this, consider how the boxed Q–Q plot in Fig. 3 shows that the censoring criterion for isochron data is not appropriate for the anomaly C3 solution if C3 picks from segment P1 are included. The inappropriateness may be due to difficulty in making accurate picks on the sometimes low amplitude anomalies there, perhaps related to subsequent deformation in interactions with the SFZ, and may be expected to give rise to an inappropriate estimate of the 95% confidence ellipsoid. The volume of the 'poorly estimated' C3 confidence region, which used the P1 data, is actually quite similar (85%) to the volume of the ellipsoid presented in Table 1 and Fig. 4. This small difference illustrates the dominance of FZ data, which are the same for both C3 solutions, over the inversion and its estimated confidence regions.

The set of poles describes a relatively stable spreading system, with those for chrons C4, C3A and C3 falling slightly to the north of a tight cluster containing the earlier poles. Stage poles, calculated from the finite poles for all intervals (Table 2), populate the same region and are remarkably well clustered in consideration of the short (~1.5–2 Myr) intervals. Confidence regions were not generated for these stage poles, but would be larger than those for the finite poles; the organisation of the cluster, which during the course of the inversion process was unstable parallel to the long axes of the finite poles' confidence ellipses, and is elongated in that direction in Fig. 5, gives a suggestion of the size and shape of possible confidence regions about the stage poles. The northward drift of stage poles younger than the C4–C3A interval, however, is a stable feature during the inversion process, and is therefore likely to exist outside the effects of data uncertainty. The unaltered continuation of FZ strikes into regions older than C5AD suggests that it would be possible to describe at least part of the pre-C5AD tectonic history of the plate pair with finite and stage poles in the same region.

6. Discussion

Larter and Barker [1] suggest that the Phoenix plate may be an example of 'pivoting subduction' [23]: they hypothesise a larger slab pull force in the northeast of the plate, where the subducting lithosphere was much older than in the southwest, that created a couple to rotate it about a point to the southwest. Those authors calculated a stage pole for the interval C6A–C5C (~21–16.5 Ma) that is indeed in such a position (Fig. 4, Table 2). Stage poles calculated between the inverted-for finite parameters in this study occupy a similar setting and hence confirm and strengthen this view. Based on their closely spaced conjugate C3 anomalies in P3, Larter and Barker could not distinguish between a late stage (post-chron C3A) SW–NE propagating extinction of the Antarctic–Phoenix Ridge and late stage rotation about a very close pole to the southwest. The recent reinterpretation [2] of magnetic anomalies in the Antarctic–Phoenix system, extended here, can rule out propagating extinction, and the rotation parameters derived by inversion do indeed show the latest stage poles moving northwards. This northward drift seems to happen in such a way that the stage poles retain a presence on a projection of the active part of the trench, whose overall azimuth changes with successive ridge-crest–trench collisions southwest of the Hero FZ. I take this apparent migration as support for Larter and Barker's pivoting subduction hypothesis [1], in which the distance to the 'subduc-

tion pivot' is determined by the gradient in slab pull forces, whose azimuth changes with that of the trench and slab.

It has also been suggested that the pivoting subduction couple, due to slab pull forces, became more effective after detachment, around chron C5, of the negatively buoyant part of the subducting slab to the northeast of the Hero FZ from a younger, warmer, more buoyant part southwest of it [1]. One line of evidence for this was anomalously large difference between faster post-C5 spreading rates measured in P3 north of the Hero FZ (35 mm/yr decreasing to 25 mm/yr by extinction) and those south of FZ 'C' (27 mm/yr decreasing to 17 mm/yr by chron C4) and a second was apparent rotation of the magnetic lineations in the intervening spreading corridor. Taken on their own, these observations may as easily have resulted from a lack of complete information about asymmetry in spreading or undetected ridge jumps, but Larter and Barker preferred the interpretation in which disintegration of the subducted part of the slab played a role, because of a system-wide increase in apparent spreading rate between chrons C5 and C3 that they took as evidence for release of the sinking part of the slab. The post-C5 increase in apparent spreading rate found in [1] was suspected to have been partly also a result of inaccuracy in the best timescale available at the time, and subsequently this inaccuracy was reported [24]. Spreading rates calculated from the inversion results (Table 3) with a more modern timescale [4] show that nearly all of the acceleration can be explained as a result of timescale error. Only a modest, short-lived, increase remains between chrons C5 and C4A. This increase is not inconsistent with release of the sinking part of the slab after chron C5, but may also highlight an inadequacy in the newer timescale. Table 3 shows that spreading rates calculated south of FZ 'C' in [1] are consistent with the two-plate system in the inversion results, and that the faster rates for P3 in [1] are a result of the close spacing of young conjugate anomalies the authors preferred. Hence, based on the results of this inversion, only the apparent rotation of anomalies between the Hero and 'C' FZs remains as evidence of a departure from a two-plate system. An interpretation, following [1], of the rotation and the small, short-lived, spreading rate increase at C5 as evidence for events in the subducted part of the Phoenix plate would be a very speculative one.

The most significant kinematic changes towards the end of the Phoenix plate's life are marked reductions in spreading rate, occurring between anomalies C4 and C3A, C3A and C3, and C3 and C2A (Fig. 1c, Table 3). It is possible that these reductions are samples of a more gradually decreasing spreading rate. The onset of late stage reduction in spreading rates has been related to increased shear stresses across the SFZ [1,2]: around chron C4/C3A the modern Scotia plate first appeared all along the northern side of the SFZ due to the cessation of spreading on the West Scotia Ridge [8,9]. If this is the case, the fact that the shear stress increase seems not to have resulted in any significant alteration of the direction of Phoenix plate movement is an argument for the pre-existence of the gross trend of

Table 3
Spreading half rates calculated for intervals between the reconstruction poles in Table 1, at points on the ridge crests in P1, P2 and P3, and in the spreading corridor south of FZ 'C'

Interval	P1 (rate/2 km/Myr)	P2 (rate/2 km/Myr)	P3 (rate/2 km/Myr)	South of FZ 'C' (rate/2 km/Myr)
C3–C2A	13.9	13.3	12.3	10.6
C3A–C3	18.3	17.7	16.8	14.7
C4–C3A	22.8	21.5	19.4	15.0
C4A–C4	30.3	29.1	27.3	22.6
C5–C4A	35.4	34.1	32.0	27.3
C5A2–C5	31.6	30.7	29.2	25.6
C5AD–C5A2	37.7	36.0	33.3	27.7

the SFZ in the azimuth of absolute Phoenix plate motion. It is likely that the SFZ initially formed by relative movements between the Phoenix plate, whose 'absolute' motion was fast [1] and the much slower-moving plates on each flank of the West Scotia Ridge. Using this, and similar inferences, further work on the tectonics of this region can help to approach a better understanding of the global plate circuit: a similar inversion performed on seafloor spreading data at the West Scotia Ridge [25] can be combined with the new results presented here in order to provide the first quantitatively derived assessments of the range of possible roles played by the Scotia Sea in the Neogene global plate circuit.

Acknowledgements

This work was funded by the German Research Foundation (DFG) through Grant GO 724/2-1. It is a refinement of PhD studies done under the supervision of Professor Derek Fairhead (University of Leeds, UK) and Dr Roy Livermore (British Antarctic Survey (BAS)) as part of the NERC Antarctic Special Topic Project GT22/95/ANT4/3. Steve Cande, Rob Larter and Dietmar Müller reviewed the manuscript. I thank my colleagues Karsten Gohl (AWI) and Roy Livermore (BAS) for their careful pre-review comments. Peter Morris (BAS) produced gridded magnetic anomalies used in deriving the isochron pick set. The figures were generated using the GMT software of P. Wessel and W.H.F. Smith. *[BW]*

References

[1] R.D. Larter, P.F. Barker, Effects of ridge-crest-trench interaction on Antarctic-Phoenix spreading: forces on a young subducting plate, J. Geophys. Res. 96 (1991) 19583–19607.
[2] R.A. Livermore, J.C. Balanyá, A. Maldonado, J.M. Martínez, J. Rodríguez-Fernández, C. Sanz de Galdeano, J. Galindo-Zaldívar, A. Jabaloy, A. Barnolas, L. Somoza, J. Hernández-Molina, E. Surioàch, C. Viseras, Autopsy on a dead spreading center the Phoenix Ridge, Drake Passage, Antarctica, Geology 28 (2000) 607–610.
[3] J.P. Kennett, Cenozoic evolution of Antarctic glaciation, the circum-Antarctic ocean and their impact on global paleoceanography, J. Geophys. Res. 82 (1977) 3843–3860.
[4] S.C. Cande, D.V. Kent, Revised calibration of the geomagnetic polarity time scale for the late Cretaceous and Cenozoic, J. Geophys. Res. 81 (1995) 4157–4162.
[5] S.C. Cande, C.A. Raymond, J. Stock, W.F. Haxby, Geophysics of the Pitman Fracture Zone and Pacific-Antarctic plate motions during the Cenozoic, Science 270 (1995) 947–953.
[6] S.C. Cande, E.M. Herron, B.R. Hall, The early Cenozoic tectonic history of the southeast Pacific, Earth Planet. Sci. Lett. 57 (1982) 63–74.
[7] R.A. Livermore, D. McAdoo, K. Marks, Scotia Sea tectonics from high-resolution satellite gravity, Earth Planet. Sci. Lett. 123 (1994) 255–268.
[8] G. Eagles, 2000. Modelling Plate Kinematics in the Scotia Sea, PhD Thesis, University of Leeds.
[9] T. Thomas, R.A. Livermore, F. Pollitze, 2003. Motion of the Scotia Sea plates, Geophys. J. Int. (in press).
[10] A.P. Nankivell, 1997. Tectonic Evolution of the Southern Ocean between Antarctica, South America and Africa over the last 84 Ma, PhD Thesis, University of Oxford.
[11] P.R. Shaw, S.C. Cande, High resolution inversion for south Atlantic plate kinematics using joint altimeter and magnetic anomaly data, J. Geophys. Res. 95 (1990) 2625–2644.
[12] P.R. Shaw, Investigations of relative plate motions in the South Atlantic using Seasat altimeter data, J. Geophys. Res. 92 (1987) 9363–9375.
[13] S.J. Hellinger, The uncertainties of finite rotations in plate tectonics, J. Geophys. Res. 86 (1981) 9312–9318.
[14] P.F. Barker, Plate tectonics of the Scotia Sea region, Nature 228 (1970) 1293–1296.
[15] M.J. Hole, R.D. Larter, Trench-proximal volcanism following ridge crest-trench collision along the Antarctic Peninsula, Tectonics 12 (1993) 897–910.
[16] D.T. Sandwell, W.H.F. Smith, Marine gravity anomaly from Geosat and ERS 1 satellite altimetry, J. Geophys. Res. 102 (1997) 10039–10054.
[17] B.H. Kirkwood, J.-Y. Royer, T.C. Chang, R.G. Gordon, Statistical tools for estimating and combining finite rotations and their uncertainties, Geophys. J. Int. 137 (1999) 408–428.
[18] C. Gaina, R.D. Müller, J.-Y. Royer, J. Stock, J. Hardebeck, P. Symonds, The tectonic history of the Tasman Sea: a puzzle with 13 pieces, J. Geophys. Res. 103 (1998) 12413–12433.
[19] R.D. Müller, D.T. Sandwell, B.E. Tucholke, J.G. Sclater, P.R. Shaw, Depth to basement and geoid expression of the Kane Fracture Zone: a comparison, Mar. Geophys. Res. 13 (1991) 105–129.
[20] T. Chang, On the statistical properties of estimated rotations, J. Geophys. Res. 92 (1987) 6319–6329.
[21] D.S. Wilson, Confidence intervals for motion and deformation of the Juan de Fuca plate, J. Geophys. Res. 98 (1993) 16053–16071.
[22] J.B. Minster, T.H. Jordan, P. Molnar, E. Haines, Numer-

ical modelling of instantaneous plate tectonics, Geophys. J. R. Astron. Soc. 36 (1974) 541–576.
[23] H.W. Menard, Fragmentation of the Farallon plate by pivoting subduction, J. Geol. 86 (1978) 99–110.
[24] A. Maldonado, R.D. Larter, F. Aldaya, Forearc tectonic evolution of the South Shetland margin, Antarctic Peninsula, Tectonics 13 (1994) 1345–1370.
[25] G. Eagles, R.A. Livermore, J.D. Fairhead, P. Morris, in preparation. Tectonics of the west Scotia Sea.